

# Tuning the indistinguishability of photons from a solid state two-level system

R. Proux, M. Maragkou, E. Baudin, C. Voisin, Ph. Roussignol, and C. Diederichs<sup>1</sup>

Laboratoire Pierre Aigrain, Ecole Normale Supérieure, CNRS, Université Pierre et Marie Curie, Université Paris Diderot, 24 rue Lhomond, 75231 Paris Cedex 05, France

**Manipulating Fock states in a solid state environment is a milestone towards the development of scalable quantum information systems<sup>1,2</sup> from a fundamental and applied research point of view. Such an implementation relies on a source of flying qubits encoded on single indistinguishable photons, able to violate Bell's inequalities and demonstrate entanglement.<sup>3,4</sup> In solid state systems such as semiconductor quantum dots (QD), photon indistinguishability is either limited by the QD dynamics under pulsed excitation,<sup>5</sup> or by the temporal resolution of the detectors under continuous wave (cw) excitation.<sup>6,7</sup> Here, we study the indistinguishability of photons emitted by a cw resonantly-driven single QD, operated below the so-called radiative limit. In this regime, the spectrum linewidth is governed by the laser coherence time<sup>3,9,10</sup> and can therefore be tuned at will, the laser coherence time becoming a free controllable parameter of the device. We show with Hong-Ou-Mandel (HOM) type experiments<sup>11</sup> that photon indistinguishability is limited neither by the QD dynamics nor the detection system time response, and can be tuned by the excitation source, enabling an unprecedented level of control.**

Indistinguishability refers to the ability of photons with similar spectral, spatial and polarization properties to bunch when arriving simultaneously on two opposite sides of a beamsplitter (BS). This coalescence effect is commonly studied by performing two-photon interference measurements in a HOM type experiment.<sup>11</sup> It relies on a Mach-Zehnder (MZ) interferometer where the intensity correlation function is measured between detectors placed at its two output channels. In the case of a two-level system excited by two consecutive pulses, perfect temporal matching between the photons arrival times at the BS where interferences occur (ensured by a precise matching of the MZ optical lengths) is mandatory for the observation of the so-called HOM dip:<sup>11</sup> a drop in the joint photodetection probability due to photon coalescence. For realistic and relatively slow detectors compared to the pulse duration, photon indistinguishability is tightly linked to the coherence time  $T_2$  and the lifetime  $T_1$  of the two-level system since perfect coalescence, and therefore a vanishing value in the HOM dip, is only observed if the radiative limit  $T_2 = 2T_1$  is reached.<sup>5</sup> The figure of merit under pulsed excitation is thus given by the ratio  $T_2/2T_1$  which constitutes a fundamental limit

to the coalescence efficiency.

In the case of cw excitation, there is no need for perfect temporal matching, but the detection system play a major role since the two-photon interference visibility related to the coalescence efficiency is governed by its temporal resolution  $T_R$ . In fact, the joint photodetection perfectly vanishes at zero time delay between two ideal ultrafast detectors, even for deviations in the photons properties such as their energies.<sup>12</sup> On the contrary, real detectors, with  $T_R > T_1, T_2$ , strongly reduce the two-photon interference visibility. Therefore, the temporal indistinguishability of the photons is only ensured if their coherence time is longer than  $T_R$ ,<sup>13</sup> and the lack of fast detectors is thus obviously a serious limitation for any implementation towards an operating device. Moreover, as the value of the intensity correlation function at zero delay is mostly determined by  $T_R$ , it cannot on its own characterize accurately the photon indistinguishability of a cw source.

In solid state, single QDs are promising atom-like systems with dynamics approaching the radiative limit. They suffer nevertheless from the interaction with their environment which tends to decrease  $T_2$ <sup>14,15</sup> and lower the indistinguishability of the emitted photons.<sup>5</sup> In this context, several strategies have been followed to approach the radiative limit. The two most successful ones are the exploitation of the Purcell effect in order to reduce  $T_1$ ,<sup>16</sup> or the use of strictly resonant excitation in order to reduce the dephasing mechanisms and thus increase  $T_2$ .<sup>17</sup> Since the first HOM experiment under pulsed excitation of Santori et al.,<sup>18</sup> where large indistinguishabilities were measured using the Purcell effect, photon indistinguishability has been investigated in resonantly-driven QDs either under pulsed<sup>19,20</sup> or cw excitation.<sup>21,22</sup> In the first case, the increase of  $T_2$  leads to a breakthrough in the generation of on-demand highly indistinguishable photons.<sup>19</sup> In the latter case however, even though photon indistinguishability is improved, the detection time response remains the major limiting factor.

In such a context, recent experimental studies have been conducted in the low excitation regime of Resonant Rayleigh Scattering (RRS) under cw excitation, where photons are elastically scattered by the QD.<sup>3,9,10</sup> As shown by homodyne detection experiments,<sup>10,20</sup> the emitted photons inherit the coherence time of the excitation laser  $T_L$ , which can be much longer than  $T_2$  and  $T_R$ , while still exhibiting sub-Poissonian statistics.<sup>3,9</sup> The resulting QD emission spectrum can then be much narrower than the natural linewidth imposed by the radiative limit, even if, as it can be seen in figure 1b, the

<sup>1</sup>email: carole.diederichs@lpa.ens.fr

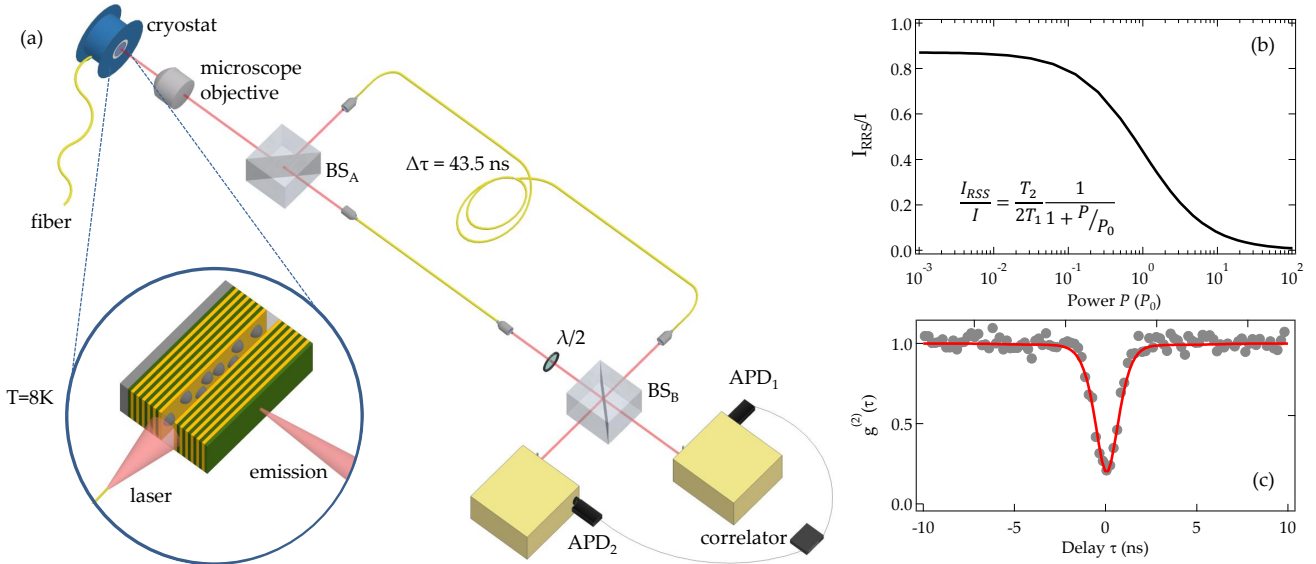


FIGURE 1 | **Experimental setup for two-photon interference and resonance fluorescence characteristics.** **a**, Illustration of the unbalanced Mach-Zehnder interferometer for two-photon interference measurements. The QD emission is split by a first beamsplitter ( $BS_A$ ) in two paths of different lengths and recombined at a second one ( $BS_B$ ). Single mode polarization maintaining fibres ensure high spatial overlap at  $BS_B$  and a half-waveplate  $\lambda/2$  controls the mutual polarization degree between the two interferometer arms. Photodetection is monitored by two avalanche photodiodes (APDs) placed at the  $BS_B$  outputs, combined with spectrometers for spectral filtering and a correlator for the intensity correlation function measurement. (inset) Orthogonal excitation-detection geometry where a QD is excited via a fibre positioned at the edge of the sample while its emission is collected by a microscope objective in an orthogonal configuration. **b**, Power dependence of the RRS intensity ratio with respect to the total QD emission intensity. The excitation power  $P$  is given in units of the optical transition saturation power  $P_0$ ,  $T_1 = 300$  ps and  $T_2 = 500$  ps. **c**, Intensity correlation function for  $P = 0.1P_0$ , fitted by Eq. 2 (see Methods), convoluted by the IRF.

ratio of the elastically scattered photons remains limited to  $T_2/2T_1$ . Considering that the inherited coherence time is surpassing  $T_R$  and Mandel's notion that coherence and indistinguishability are heavily entwined,<sup>23</sup> the RRS regime constitutes the ideal ground for the investigation of the generation of highly indistinguishable photons and also offers a means of controlling this indistinguishability by changing the excitation laser coherence time.

Here, resonant excitation of the excitonic fundamental transition of a single InAs/GaAs QD (see Methods for sample details and Supplementary Information SII for details on the QD emission characterization) is achieved in an orthogonal excitation-detection geometry,<sup>3,24</sup> using a cw tunable external cavity diode laser with variable coherence time (see SI2). The QD emission is sent to a MZ interferometer (see Fig. 1a). Varying the path difference makes the interferometer balanced (unbalanced) for one (two)-photon interference measurements. In order to prevent fictitious anti-coincidences from one-photon interference when performing two-photon interference (see SI3), the path difference in the unbalanced MZ interferometer must be larger than the photon coherence time and thus larger than  $T_L$  in the RRS regime. This is ensured by a 10 m long optical fibre which corresponds to a delay  $\Delta\tau = 43.5$  ns. A half-wave plate inserted in the interferometer short path is used to change the respective photons polarization, making them mutually parallel or orthogonally polarized. By blocking one arm, the setup becomes a Hanbury Brown and Twiss (HBT) setup for measuring the intensity correlation function  $g^{(2)}(\tau)$ ,

where  $\tau$  is the electronic delay between the two detectors, and establishing the QD emission statistics.

The instrument response function (IRF) measured in the HOM setup has a FWHM of  $T_R = 1$  ns (see SI3). The QD exciton lifetime  $T_1 = 300$  ps and the coherence time  $T_2 = 500$  ps are independently measured under resonant excitation (see SI4). Figure 1c presents the intensity correlation function measured with the HBT setup at an excitation power  $P$  well below the saturation power of the optical transition  $P_0$  ( $P = 0.1P_0$ ), fitted by the  $g^{(2)}$  function of a resonantly excited two-level system (see Methods, Eq. 2), convoluted by the IRF. An antibunching is observed with  $g^{(2)}(0) = 0.21$ , demonstrating that the QD is a single photon source in the RRS regime.

Figures 2a-d present two examples of the intensity correlation function measured in the HOM setup when the photons have mutual orthogonal (Fig. 2a,b) and parallel (Fig. 2c,d) polarizations, for  $P = 0.17P_0$  (Fig. 2a,c) and  $P = 1.27P_0$  (Fig. 2b,d), and  $T_L = 16$  ns. The experimental data (grey dots) are fitted (red solid line) by the theoretical intensity correlation functions<sup>6</sup>  $g_{\parallel}^{(2X)}$  and  $g_{\perp}^{(2X)}$  given by Eq. 5 and 6 (see Methods), respectively. All the following fits are convoluted by the IRF and all the experimental data are fitted with the same set of parameters. The measured parameters are the reflection and transmission intensity coefficients of the beamsplitters  $BS_{A(B)}$ ,  $R_{A(B)} = 0.45$  and  $T_{A(B)} = 0.55$ , respectively;  $T_1 = 300$  ps and  $T_2 = 500$  ps; and  $\Delta\tau = 43.5$  ns. The parameter including all experimental imperfections

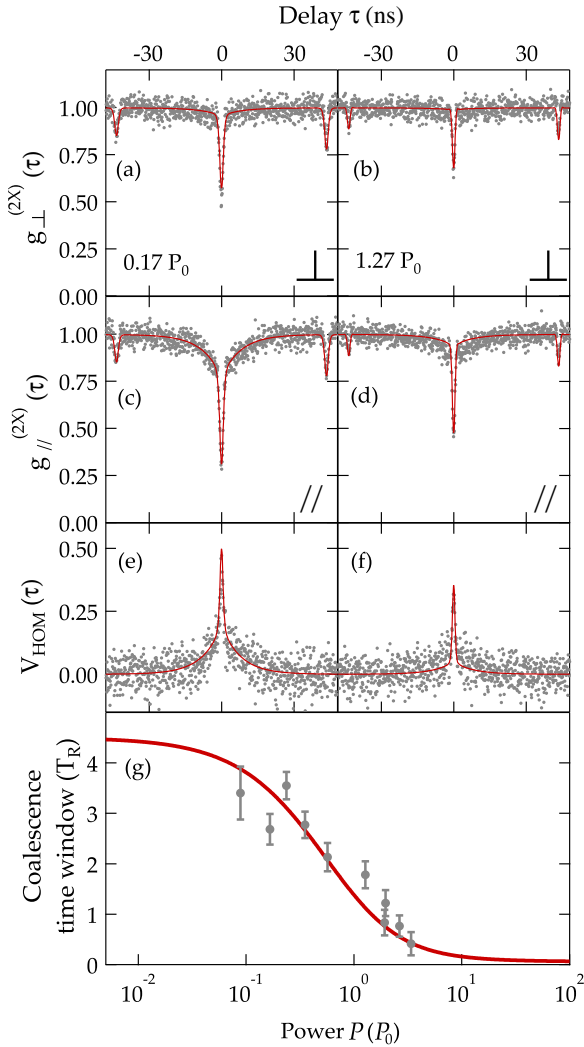


**FIGURE 2 | Photon indistinguishability versus the excitation power.** **a,b**, Two-photon interference measurements for orthogonally polarized photons below saturation ( $P = 0.17P_0$ ) and slightly above saturation ( $P = 1.27P_0$ ), respectively. **c,d**, Same measurements as **a** and **b** for parallel polarized photons. **e,f**, Two-photon interference visibility at  $P = 0.17P_0$  and  $P = 1.27P_0$ , respectively. The experimental data (grey dots) are fitted (red solid line) by Eq. 6 for **a,b**, Eq. 5 for **c,d** and Eq. 7 for **e,f** (see Methods for equations). All the fits are convoluted by the IRF. **g**, Coalescence time window deduced from the experimental (grey dots) and theoretical (red solid line) visibilities as a function of the excitation power  $P$  (units  $P_0$ ).

(polarization, alignment, background) that can possibly destroy the perfect overlap in space or polarization of the two beams at  $BS_B$  is extracted from the fits and equals  $V_0 = 0.8$  (0.15) for parallel (orthogonal) polarization.

For mutually orthogonal and therefore distinguishable photons (see Fig. 2a,b), no coalescence phenomenon is expected and the measured  $g_{\perp}^{(2X)}$  function is related to the statistical properties of the single photon source when light is sent to the MZ interferometer. Compared to an HBT experiment, additional antibunching dips shifted by the interferometer path difference are observed at

$\tau = \pm\Delta\tau$ , and the three measured dip values are only resolution limited. Note that above saturation (see Fig. 2b), the QD undergoes Rabi oscillations (see SI4), inducing a narrowing of the antibunching dips<sup>25</sup> and thus a strong reduction of the dip visibility for a given  $T_R$ . For mutually parallel photons (see Fig. 2c,d), apart from the contribution of the photon statistics, an additional component due to photon coalescence is observed. Below saturation (see Fig. 2c), two dynamics can be distinguished: a fast one at  $\tau \ll T_R$  characterized by the intrinsic QD time constants  $T_1$  and  $T_2$ , and a much slower one characterized by  $T_L$ . This demonstrates that the additional coalescence component is directly linked to the  $g^{(1)}$  function and thus to the coherence of the emitted photons. The fast dynamics then reflects the photon statistics and the coalescence of the inelastically scattered photons, whereas the slower one is directly linked to the coalescence of the elastically scattered photons. However, as expected, above saturation (see Fig. 2d), the long time component vanishes along with the ratio of the elastically scattered photons (see Fig. 1b).

Figures 2e,f present the experimental (grey dots) and theoretical (red solid line) two-photon interference visibilities  $V_{\text{HOM}}(\tau) = [g_{\perp}^{(2X)}(\tau) - g_{\parallel}^{(2X)}(\tau)]/g_{\perp}^{(2X)}(\tau)$  below and above saturation, respectively. In order to take into account the long coherence time of the elastically scattered photons along with the visibility value at  $\tau = 0$ , we believe that a more appropriate figure of merit than only the value of  $V_{\text{HOM}}(0)$  should be used. The time integration of the visibility curve, or what we call the coalescence time window, is thus chosen as the figure of merit under cw excitation in order to investigate the temporal behavior of the coalescence efficiency. Moreover, when given in units of  $T_R$ , it allows for a direct comparison with the temporal resolution of the detectors. Figure 2g shows the power dependence of the coalescence time window, where the experimental results (grey dots) are in agreement with the theoretical values (solid red line) calculated from Eq. 7 (see Methods). Below saturation, the coalescence time window can be as large as  $4T_R$  due to the QD coherence properties inherited from the excitation laser in the RRS regime. At saturation, the coalescence time window is drastically reduced to  $T_R$  since at this excitation power the QD emission mostly originates from inelastic scattering (see Fig. 1b) and the QD dynamics is governed by the intrinsic time constants  $T_1$  and  $T_2$  which are of the order of  $T_R$ . As a comparison, the coalescence time window calculated for a non-resonantly excited QD with the same time constants  $T_1$  and  $T_2$  equals  $0.15T_R$ , which is similar to the one measured above saturation ( $0.4T_R$  at  $P = 5P_0$ ). We conclude that operating in the low power RRS regime allows for coalescence to occur for time delays up to 4 times the temporal resolution of the detectors. We stress that these coalescence time windows can only be observed because of the slow dynamics with respect to the detectors response time in the particular RRS regime.

Figure 3a presents the two-photon interference visibilities for various laser coherence times  $T_L$  when the QD operates in the RRS regime below saturation ( $P=0.3P_0$ ).

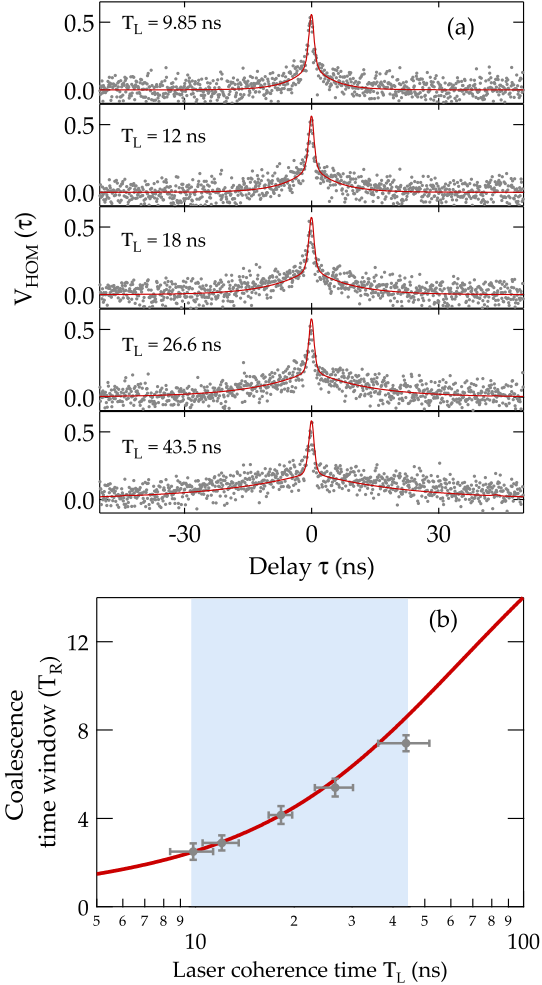


FIGURE 3 | **Photon indistinguishability versus the excitation laser coherence time** **a**, Two-photon interference visibility for various laser coherence times  $T_L$ , at  $P = 0.3P_0$ . Experimental data (grey dots) are shown with the corresponding fits (red solid line) given by Eq. 7 (see Methods) and convoluted by the IRF. **b**, Coalescence time window as a function of the laser coherence time  $T_L$ . The experimental data (grey dots) are fitted (solid red line) by the theoretical values calculated from Eq. 7 (see Methods), convoluted by the IRF. The shaded area corresponds to the reachable range of  $T_L$  set by the experimental conditions.

The experimental data (grey dots) are fitted (red solid line) by Eq. 7 (see Methods). The experimental conditions set the reachable range of  $T_L$ , where the minimum achievable value is  $T_L = 9.85$  ns (see SI2), and the maximum value  $T_L = 43.5$  ns is imposed by the interferometer delay  $\Delta\tau$ . With the ratio of the elastically scattered photons being constant at a given power ( $I_{RRS}/I \approx 70\%$  at  $P = 0.3P_0$ ), an increase of  $T_L$  is directly reflected on the slow component of the visibility. The corresponding coalescence time windows are presented as a function of  $T_L$  in figure 3b. The experimental data (grey dots) are in agreement with the theoretical values (solid red line) calculated from Eq. 7 (see Methods). Note that these theoretical values can be calculated within the present

model only if  $T_L > T_1, T_2$  (domain of validity of the rotating wave approximation made to express the correlation functions  $g^{(1)}$  and  $g^{(2)}$  characterizing a resonantly excited two-level system). When  $T_L < T_1, T_2$ , the coalescence time window is imposed by  $T_1$  and  $T_2$  as in the resonant pulsed excitation case. However, the increase of the coalescence time windows is directly related to the increase of  $T_L$ , resulting in a value up to  $8T_R$  with the current setup. Therefore, in the case of RRS, photon indistinguishability is limited neither by the intrinsic QD time constants nor  $T_R$ , and the higher the laser coherence time, the higher the coalescence time window. This result not only demonstrates that coherence and indistinguishability are tightly entwined,<sup>23</sup> but also that the RRS regime allows for an unprecedented level of control of photon indistinguishability. Furthermore, the limit of the maximum possible indistinguishability is mainly imposed by the excitation laser. Moreover, even if reaching the radiative limit would improve the ratio of the elastically scattered photons and thus the coalescence time window ( $\sim 20\%$  in our case), the criteria  $T_2 = 2T_1$  is not an unavoidable limit anymore.

In this Letter, we have demonstrated the generation of highly indistinguishable single photons from a resonantly-driven QD operated in the RRS regime. In all experiments performed so far with single QDs, the coherence time of the emitted photons was of the order of the temporal resolution of the detectors, so that the temporal profile of photon indistinguishability could not be resolved. In the RRS regime, because the excitation laser drives the photon coherence time, one can experimentally investigate the temporal dynamics of the photon coalescence phenomenon. Then, a more appropriate figure of merit has to be defined in order to quantify the time window in which two-photon coalescence is observable. We have shown that this coalescence time window can be fully tuned by the excitation laser in the RRS regime and can be as large as 8 ns in the present setup (compared to 0.15 ns for a non-resonantly excited QD, or 0.4 ns for a resonantly-driven QD above saturation). We point out that this level of control could be further exploited in a Franson type interferometer for the generation under cw excitation of time-bin entangled states out of two single photons.<sup>26</sup> In such a scheme, as the coalescence time window exceeds the temporal resolution of regular detectors, a precise timing of the photons could be ensured without the use of narrow spectral filters or superconducting detectors, which would then allow to implement time entanglement of photon pairs.<sup>27,28</sup>

## Methods

**Sample details and setup collection efficiency.** The InAs/GaAs self-assembled QDs under study are embedded in a planar  $\lambda_0$ -GaAs microcavity formed by two distributed-Bragg reflectors of 11 and 24 pairs of  $\lambda_0/4$  layers of AlAs and AlGaAs, respectively. The sample is maintained at low temperature (8K) in a Helium continuous flow cold finger cryostat. By means of the microcavity, an extraction efficiency of about 10% is reached. Taking into account the transmission of the microscope objective (63%), the beamsplitters (90%) and the polarizing elements (70%), about 50% of these photons arrive in the interferometer, which has an overall efficiency of 66.5% (70% fibre coupling and 95% for  $BS_A$  and  $BS_B$ ). The overall efficiency of the gratings in the spectrometers and the APDs is

not more than 7%. Despite a resulting overall efficiency of 0.25%, 10 000 counts/s are typically detected on each APD when working below saturation ( $P \ll P_0$ ). These detection levels are comparable to the emission rates measured for QD-based single photon sources where the photon extraction and collection efficiencies are optimized.<sup>29</sup>

**Equations under resonant excitation.** For a two level system under resonant excitation, the first- and second-order correlation functions  $g^{(1)}$  and  $g^{(2)}$  are given by:

$$g^{(1)}(\tau) = e^{-\tau/T_L} \left[ \frac{T_2}{2T_1} \cdot \frac{1}{1 + \Omega^2 T_1 T_2} + \frac{e^{-\tau/T_2}}{2} + \frac{e^{-\eta\tau}}{2} \left( \tilde{\alpha} \cos(\nu\tau) + \tilde{\beta} \sin(\nu\tau) \right) \right] \quad (1)$$

and

$$g^{(2)}(\tau) = 1 - e^{-\eta\tau} \left( \cos(\nu\tau) + \frac{\eta}{\nu} \sin(\nu\tau) \right) \quad (2)$$

with

$$\begin{cases} \eta = \frac{1}{2} \left( \frac{1}{T_1} + \frac{1}{T_2} \right) \\ \nu = \sqrt{\Omega^2 - \frac{1}{4} \left( \frac{1}{T_1} - \frac{1}{T_2} \right)^2} \\ \tilde{\alpha} = 1 - \frac{T_2}{T_1(1 + \Omega^2 T_1 T_2)} \\ \tilde{\beta} = \frac{\Omega^2 T_1 (3T_2 - T_1) - \frac{(T_1 - T_2)^2}{T_1 T_2}}{2\nu T_1 (1 + \Omega^2 T_1 T_2)} \end{cases} \quad (3)$$

$\tau$  is the delay between detections,  $T_L$  the coherence time of the resonant excitation laser ( $T_L > T_1, T_2$ ), and  $\Omega$  the Rabi frequency defined as:

$$\Omega^2 = \frac{P}{P_0} \frac{1}{T_1 T_2} \quad (4)$$

The two-photon interference experimental data measured in the HOM interferometer are fitted using:<sup>6</sup>

$$g_{//}^{(2X)}(\tau) = \frac{1}{N} \left[ 4(T_A^2 + R_A^2)R_B T_B g^{(2)}(\tau) + 4R_A T_A \left( T_B^2 g^{(2)}(\tau - \Delta\tau) + R_B^2 g^{(2)}(\tau + \Delta\tau) - 4R_A T_A (T_B^2 + R_B^2) V_0 |g^{(1)}(\tau)|^2 \right) \right] \quad (5)$$

where  $N = 4R_A T_A (R_B^2 + T_B^2) + 4R_B T_B (R_A^2 + T_A^2)$  is a normalizing factor,  $R_{A(B)}$  and  $T_{A(B)}$  are the reflection and transmission intensity coefficients of the beamsplitters  $BS_{A(B)}$  respectively, and  $\Delta\tau$  is the delay between the two paths of the MZ interferometer.  $V_0$  is a parameter including all experimental imperfections that can possibly destroy the perfect overlap of the two beams at  $BS_B$  (alignment, polarization, background). When photons are perfectly mutually orthogonal (i.e.  $V_0 = 0$ ), no interference can be observed (i.e. the last term of  $g_{//}^{(2X)}$  disappears) and:

$$g_{\perp}^{(2X)}(\tau) = \frac{1}{N} \left[ 4(T_A^2 + R_A^2)R_B T_B g^{(2)}(\tau) + 4R_A T_A \left( T_B^2 g^{(2)}(\tau - \Delta\tau) + R_B^2 g^{(2)}(\tau + \Delta\tau) \right) \right] \quad (6)$$

The two-photon interference visibility is defined as:

$$V_{\text{HOM}}(\tau) = \frac{g_{\perp}^{(2X)}(\tau) - g_{//}^{(2X)}(\tau)}{g_{\perp}^{(2X)}(\tau)} \quad (7)$$

We stress that equations 5 and 6 depend on the first- and second-order correlation functions  $g^{(1)}$  and  $g^{(2)}$  of a resonantly excited two-level system, given by Eq. 1 and 2, respectively. Both  $g^{(1)}$  and  $g^{(2)}$  functions are significantly different with respect to the non-resonant case since they both depend on  $T_1$  and  $T_2$ , resulting in more complex dynamics for  $g_{//}^{(2X)}$  and  $g_{\perp}^{(2X)}$  under resonant excitation.

## References

- <sup>1</sup> M. A. Nielsen & I. L. Chuang, *Quantum Computation and Quantum Information* Cambridge University Press, (2000).
- <sup>2</sup> N. Gisin, G. Ribordy, W. Tittel, & H. Zbinden, *Quantum cryptography*, Rev. Mod. Phys. **74**, 145 (2002).
- <sup>3</sup> W. Tittel, J. Brendel, N. Gisin & H. Zbinden, *Long-distance Bell-type tests using energy-time entangled photons*, Phys. Rev. A **59**, 4150-4163 (1999).
- <sup>4</sup> D. Fattal, K. Inoue, J. Vuckovic, C. Santori, G. S. Solomon, & Y. Yamamoto, *Entanglement Formation and Violation of Bell's Inequality with a Semiconductor Single Photon Source*, Phys Rev Lett. **92**, 037903 (2004).
- <sup>5</sup> J. Bylander, I. Robert-Philip & I. Abram, *Interference and correlation of two independent photons*, Eur. Phys. J. D **22**, 295-301 (2002).
- <sup>6</sup> R. B. Patel, A. J. Bennett, K. Cooper, P. Atkinson, C. A. Nicoll, D. A. Ritchie, & A. J. Shields, *Postselective Two-Photon Interference from a Continuous Nonclassical Stream of Photons Emitted by a Quantum Dot*, Phys. Rev. Lett. **100**, 207405 (2008).
- <sup>7</sup> R. B. Patel, A. J. Bennett, I. Farrer, C. A. Nicoll, D. A. Ritchie & Andrew J. Shields, *Two-photon interference of the emission from electrically tunable remote quantum dots*, Nature Photon. **4**, 632 (2010); and Supplementary information.
- <sup>8</sup> H. S. Nguyen, G. Sallen, C. Voisin, Ph. Roussignol, C. Diederichs & G. Cassabois, *Ultra-coherent single photon source*, Appl. Phys. Lett. **99**, 261904 (2011).
- <sup>9</sup> C. Matthiesen, A. Nickolas Vamivakas, & M. Atatüre, *Subnatural Linewidth Single Photons from a Quantum Dot*, Phys. Rev. Lett. **108**, 093602 (2012).
- <sup>10</sup> K. Konthasinghe, J. Walker, M. Peiris, C. K. Shih, Y. Yu, M. F. Li, J. F. He, L. J. Wang, H. Q. Ni, Z. C. Niu, & A. Muller, *Coherent versus incoherent light scattering from a quantum dot*, Phys. Rev. B **85**, 235315 (2012).
- <sup>11</sup> C. K. Hong, Z. Y. Ou & L. Mandel, *Measurement of subpicosecond time intervals between two photons by interference*, Phys. Rev. Lett. **59**, 18, 2044-2046, (1987).
- <sup>12</sup> T. Legero, T. Wilk, M. Hennrich, G. Rempe & A. Kuhn, *Quantum beat of two single photons*, Phys. Rev. Lett. **93**, 070503 (2004).
- <sup>13</sup> M. Halder, A. Beveratos, R. T. Thew, C. Jorel, H. Zbinden & N. Gisin, *High coherence photon pair source for quantum communication*, New Journal of Physics **10**, 023027 (2008).
- <sup>14</sup> C. Kammerer, C. Voisin, G. Cassabois, C. Delalande, Ph. Roussignol, F. Klopff, J. P. Reithmaier, A. Forchel, & J. M. Gérard, *Line narrowing in single semiconductor quantum dots: Toward the control of environment effects*, Phys. Rev. B **66**, 041306(R) (2002).
- <sup>15</sup> M. Abbarchi, F. Troiani, C. Mastrandrea, G. Goldoni, T. Kuroda, T. Mano, K. Sakoda, N. Koguchi, S. Sanguinetti, A. Vinattieri, & M. Gurioli, *Spectral diffusion and line broadening in single self-assembled GaAs/AlGaAs quantum dot photoluminescence* Applied Physics Letters **93**, 162101 (2008).
- <sup>16</sup> J. M. Gérard, B. Sermage, B. Gayral, B. Legrand, E. Costard, & V. Thierry-Mieg, *Enhanced Spontaneous Emission by Quantum Boxes in a Monolithic Optical Microcavity*, Phys. Rev. Lett. **81**, 1110-1113 (1998).
- <sup>17</sup> A. Muller, E. B. Flagg, P. Bianucci, X. Y. Wang, D. G. Deppe, W. Ma, J. Zhang, G. J. Salamo, M. Xiao, & C. K. Shih, *Resonance Fluorescence from a Coherently Driven Semiconductor Quantum Dot in a Cavity*, Phys. Rev. Lett. **99**, 187402 (2007).
- <sup>18</sup> C. Santori, D. Fattal, J. Vuckovic, G. S. Solomon, & Y. Yamamoto, *Indistinguishable photons from a single-photon device*, Nature **419**, 594 (2002).
- <sup>19</sup> Y.-M. He, Y. He, Y.-J. Wei, D. Wu, M. Atatüre, C. Schneider, S. Hofling, M. Kamp, C.-Y. Lu & J.-W. Pan, *On-demand semiconductor single-photon source with near-unity indistinguishability* Nature Nanotech. **8**, 213-217 (2013).

- <sup>20</sup> C. Matthiesen, M. Geller, C. H. H. Schulte, C. Le Gall, J. Hansom, Z. Li, M. Hugues, E. Clarke, & M. Atature, *Phase-locked indistinguishable photons with synthesized waveforms from a solid-state source*, Nature Commun. **4**, 1600 (2013).
- <sup>21</sup> S. Ates, S. M. Ulrich, S. Reitzenstein, A. Löffler, A. Forchel, & P. Michler, *Post-Selected Indistinguishable Photons from the Resonance Fluorescence of a Single Quantum Dot in a Microcavity*, Phys. Rev. Lett. **103**, 167402 (2009).
- <sup>22</sup> K. Konthasinghe, M. Peiris, Y. Yu, M. F. Li, J. F. He, L. J. Wang, H. Q. Ni, Z. C. Niu, C. K. Shih, & A. Muller *Field-Field and Photon-Photon Correlations of Light Scattered by Two Remote Two-Level InAs Quantum Dots on the Same Substrate*, Phys. Rev. Lett. **109**, 267402 (2012).
- <sup>23</sup> L. Mandel, *Coherence and indistinguishability*, Optics Letters, Vol. **16**, Issue 23, 1882-1883 (1991).
- <sup>24</sup> H. S. Nguyen, G. Sallen, C. Voisin, Ph. Roussignol, C. Diederichs & G. Cassabois, *Optically Gated Resonant Emission of Single Quantum Dots*, Phys. Rev. Lett. **108**, 057401 (2012).
- <sup>25</sup> E. B. Flagg, A. Muller, J. W. Robertson, S. Founta, D. G. Deppe, M. Xiao, W. Ma, G. J. Salamo & C. K. Shih, *Resonantly driven coherent oscillations in a solid-state quantum emitter*, Nature Phys. **5**, 203 - 207 (2009).
- <sup>26</sup> M. Laroqué, A. Beveratos & I. Robert-Philip, *Entangling single photons on a beamsplitter*, Eur. Phys. J. D **47**, 119–125 (2008).
- <sup>27</sup> M. Zukowski, A. Zeilinger, M. A. Horne & A. K. Ekert, *"Event-Ready-Detectors" Bell experiment via Entanglement Swapping*, Phys. Rev. Lett. **71**, 4287 (1993).
- <sup>28</sup> M. Halder, A. Beveratos, N. Gisin, V. Scarani, C. Simon & H. Zbinden, *Entangling independent photons by time measurement*, Nature Phys. **3** 10, 692-695 (2007).
- <sup>29</sup> J. Claudon, J. Bleuse, N. S. Malik, M. Bazin, P. Jaffrennou, N. Gregersen, C. Sauvan, P. Lalanne & J. M. Gérard, *A highly efficient single-photon source based on a quantum dot in a photonic nanowire*, Nat. Photonics **4**, 174 (2010).

## Acknowledgements

The authors acknowledge P. Petroff for providing the sample. The authors would like to thank A. Beveratos and E. del Valle for useful discussions. This work was supported by the ANR project EXTREME and DGA.

## Author contributions

RP and MM performed the experiments and analyzed the data, EB performed the theoretical analysis with input from CD. MM, RP and CD wrote the paper with input from all the coauthors.

# Tuning the indistinguishability of photons from a solid state two-level system

R. Proux, M. Maragkou, E. Baudin, C. Voisin, Ph. Roussignol, and C. Diederichs<sup>1</sup>

Laboratoire Pierre Aigrain, Ecole Normale Supérieure, CNRS, Université Pierre et Marie Curie, Université Paris Diderot, 24 rue Lhomond, 75231 Paris Cedex 05, France

## SI 1 Exciton fine structure splitting and polarization characterization

Figure SI 1a shows an excitation spectrum of the fundamental transition of the studied QD. The excitation laser scans spectrally the excitonic transition, while the detection is broadband, covering the whole range of the measurement — in practice, the slits of the spectrometer are wide open. The emission wavelength of the exciton is approximately 975 nm. The slope of the background corresponds to a change of the laser intensity during the scan. Because the QD axis are tilted with respect to the sample crystallographic ones,<sup>3</sup> the fine structure of the exciton is observable.

A polarizer at the input of the HOM interferometer is used to select the polarization in the detection setup. Figure SI 1b shows the polarization scans for the two peaks observed in the excitation spectrum as well as for the background laser. All the measurements in this paper were done on peak B, which allows to cross the polarizer with respect to the laser polarization while keeping a good level of signal. This maximizes the ratio between the QD emission at the energy of peak B and the scattered laser background.

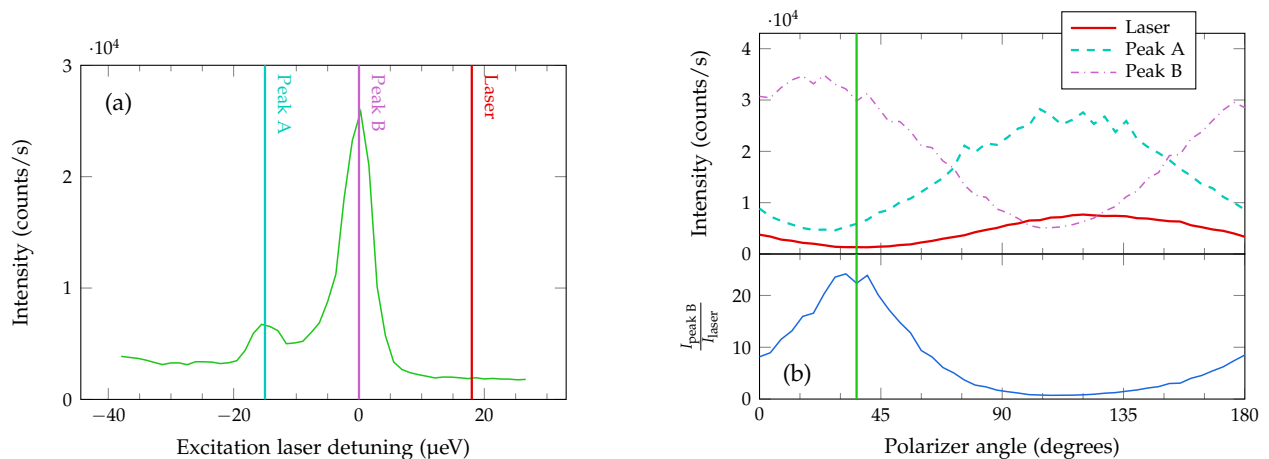


FIGURE SI 1 | **Optical properties of the excitonic transition.** **a**, Excitation spectrum (green curve) of the excitonic transition. The vertical lines represent the energies at which we performed a polarization scan (see Fig. SI 1b). **b**, Polarization scans for peaks A and B, and the laser background. The curve displayed in the bottom panel shows the intensity ratio between peak B and the laser scattering. The green line represents the polarization which was selected for our measurements.

## SI 2 Laser diode and Laser Coherence Controller

The excitation laser is an external-cavity monomode continuous wave diode laser (Toptica DL pro 940). The losses in the cavity and the longitudinal mode selection are ensured by a grating in Littrow configuration which can be rotated to tune roughly the emission wavelength between 910 nm and 985 nm. The cavity length can be finely tuned thanks to a piezoelectric actuator. The overall accuracy of the spectral relative position is less than 5 MHz, two orders of magnitude below the linewidth of the quantum dot (QD).

The electrical current passing through the diode laser can be modulated by a noise generator (Toptica Laser Coherence Controller – LCC). The LCC output is a white noise of electrical current with a bandwidth in the 10 – 250 MHz range, and variable modulation power. The diode laser output is thus modulated in phase and amplitude, resulting in a broadened lorentzian spectral line.

<sup>1</sup>email: carole.diederichs@lpa.ens.fr

The coherence time of the laser emission is here defined as the decay time  $T_L$  of the exponential in the first-order correlation function  $g^{(1)}$ :

$$g^{(1)}(\tau) = e^{-|\tau|/T_L} \quad (8)$$

According to the Wiener–Khintchine theorem, the corresponding spectral power density  $S(\nu)$  is then:

$$S(\nu) \propto \frac{1}{1 + \left(\frac{2\nu}{\Delta\nu}\right)^2} \quad (9)$$

where  $\Delta\nu = 1/(\pi T_L)$  is the full width at half maximum.

The coherence time is measured with two different techniques: Fabry-Perot interferometry and  $g_{\parallel}^{(2X)}$  intensity correlation measurement at the output of the unbalanced Mach-Zehnder interferometer used for the Hong-Ou-Mandel (HOM) type experiment. The  $g_{\parallel}^{(2X)}$  function is given for a lorentzian spectrum of coherence time  $T_L$  and no amplitude fluctuations by:<sup>1</sup>

$$g_{\parallel}^{(2X)}(\tau) = 1 - \frac{1}{2} \cdot |g^{(1)}(\tau)|^2 = 1 - \frac{1}{2} \cdot e^{-2|\tau|/T_L} \quad (10)$$

As shown in figure SI 2a, these two techniques (red squares for Fabry-Perot and yellow diamonds for  $g_{\parallel}^{(2X)}$ ) show only small differences. The coherence times in the main paper were measured using the  $g_{\parallel}^{(2X)}$  method which is the most reliable one (the Fabry-Perot has a resolution of 10 MHz — of the order of the narrowest laser linewidths — and the measurement can then be altered for the highest values of the laser coherence time).

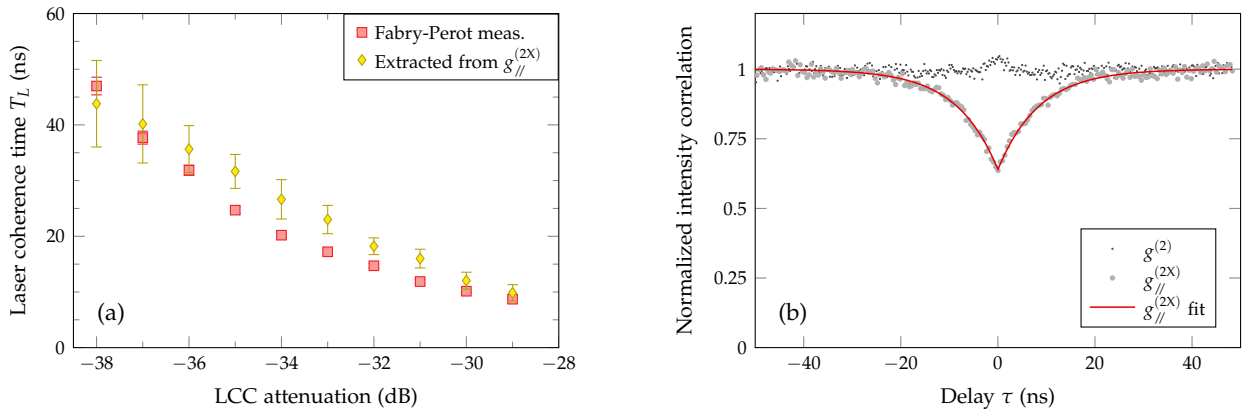


FIGURE SI 2 | **Effect of the LCC modulation attenuation on the coherence time of the excitation laser.** **a**, Coherence time of the diode laser versus the LCC attenuation (i.e. the modulation power) extracted from the Fabry-Perot measurements (red squares, deconvoluted by the Fabry-Perot response) and the  $g_{\parallel}^{(2X)}$  measurements (yellow diamonds). **b**, Experimental data (light gray dots) and fit (solid red line) of the intensity correlation function  $g_{\parallel}^{(2X)}$  when only the laser is sent to the HOM interferometer. The intensity correlation function  $g^{(2)}$ , measured in a HBT setup, is also shown (dark gray dots). The LCC attenuation is  $-31$  dB and the coherence time extracted from the fit is  $T_L = 17.0 \pm 0.5$  ns.

An example of a two-photon interference measurement performed on the laser only (i.e.  $g_{\parallel}^{(2X)}$ ) is shown in figure SI 2b (light gray dots). The quality of the theoretical fit (red solid line) demonstrates the robustness of the  $g_{\parallel}^{(2X)}$  method. However, a  $g^{(2)}$  measurement performed in a Hanbury Brown and Twiss (HBT) setup exhibits a very small bunching (dark gray dots), of the order of 3%. This is linked to the LCC process, since the  $g^{(2)}$  of a laser should read:<sup>2</sup>

$$g^{(2)}(\tau) = 1 + \text{F}[\text{RIN}] \quad (11)$$

where  $\text{F}[\text{RIN}]$  is the Fourier transform of the laser Relative Intensity Noise. Here, because of the strong modulation on the diode laser current, the amplitude of the laser emission is also affected by the modulation, and the RIN goes from 10 MHz to  $> 250$  MHz, which would correspond to a bunching less than 8 ns wide. This bunching is in fact observed on the experimental results and is about 4 ns wide. Nevertheless, this effect is very small and the excitation laser can be considered as a quite stable field as far as the detection system is concerned. We also stress that, when measured on the QD, the single photon character of the QD emission attenuates considerably the bunching effect inherent to the excitation laser since it occurs on the same time scales. Thus, this phenomenon will affect very slightly the reliability of our model equations around zero delay. In this context, the bunching effect due to the laser modulation has been neglected in all the  $g^{(2)}$  and  $g_{\parallel}^{(2X)}$  measurements presented in the paper.

## SI 3 One- and two-photon interference measurements

The difference between one- and two-photon interference, also called second- and fourth-photon interference, is what is measured in the experiment, i.e. whether detecting one or two photons.<sup>4</sup>

In the case of two-photon interference with a single source, the use of a strongly unbalanced interferometer prevents any constant phase correlation between its two outputs, or in other words it ensures the absence of one-photon interference. One could argue that the measurement of photon pairs is not altered by phenomena which modify the one-photon measurements. However, the individual rates fluctuations at the outputs of the beamsplitter will affect the visibility of the two-photon interference measurements, in addition to their influence on the coincidence rate.

Figure SI 3a shows the effect of the LCC modulation on the one-photon interference: the fringes visibility (red dots) decreases when the laser linewidth increases. This measurement was performed without fibers, with an unbalanced Michelson interferometer and a path difference of 27 ns (corresponding to 8 m). The result is consistent with the expected behavior of a lorentzian spectrum when varying the FWHM (blue solid line). Figure SI 3b shows a  $g_{//}^{(2X)}$  measurement performed with the HOM interferometer on the QD emission (in the resonant Rayleigh Scattering regime) when the laser coherence time  $T_L = 43$  ns is very close to the interferometer delay  $\Delta\tau = 43.5$  ns. This results in a long decay which reaches the secondary peaks at  $\pm\Delta\tau$ . The experimental data are fitted by equation 5 (see Methods of the main paper). We would like to stress that the model defined by equations 5 and 6 (see Methods of the main paper) cannot describe reliably the results of the HOM measurements as soon as the coherence time of the emitted photons gets longer than  $\Delta\tau$ . The detection system Instrument Response Function (IRF) of the HOM type experiment is also presented in figure SI 3b.

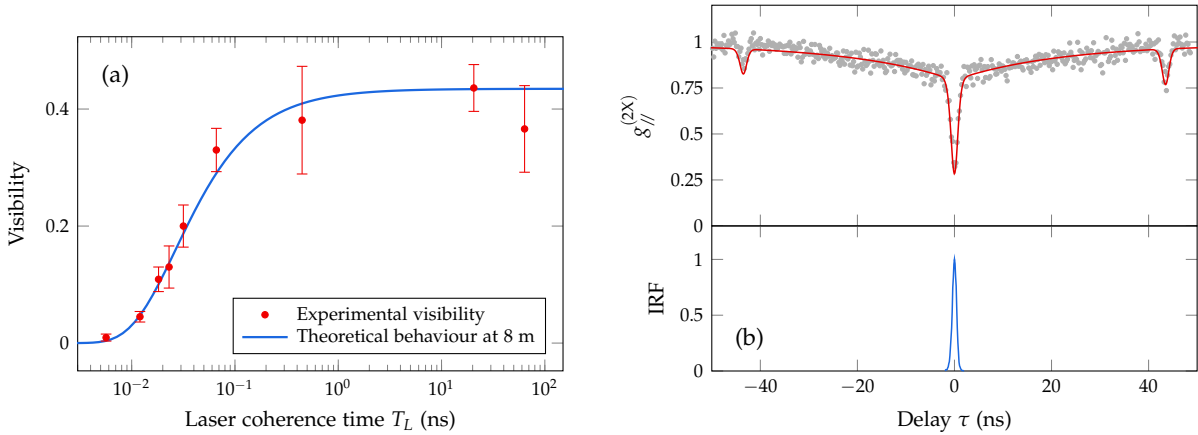


FIGURE SI 3 | **Condition on the HOM interferometer path difference for accurate two-photon interference measurements.** **a**, Visibility (red dots) of the one-photon interference fringes, measured in a Michelson interferometer with a delay of 27 ns (corresponding to 8 m), as a function of the excitation laser linewidth. The blue solid line is the expected behavior for a lorentzian spectrum at such delay. **b**, Top: Intensity correlation function  $g_{//}^{(2X)}$  measured in the HOM type experiment for  $T_L = 43$  ns (gray markers), fitted by Eq. 5 (see Methods of the main paper) (red solid curve). Bottom: Instrument Response Function of the HOM experiment (IRF, blue solid curve).

## SI 4 Dynamical properties of the quantum dot emission

Figure S4 shows two experimental results used to assess the lifetime  $T_1$  and the coherence relaxation time  $T_2$  of the two-level system model that describes the QD. All the fits presented in the paper were done with the same experimental values of  $T_1$  and  $T_2$ .

For  $T_1$ , a decay curve measurement was performed using a pulsed Ti:Sapphire laser tuned in resonance with the QD excitonic transition (see Fig. SI 4a), with a pulse width of the order of 10 ps. The IRF (dashed green line) is presented and the IRF-convoluted exponential decay used for the fit (red solid line) implies a lifetime  $T_1 = 0.34 \pm 0.05$  ns.

For  $T_2$ , a  $g^{(1)}$  measurement is performed in a balanced Mach-Zehnder interferometer by measuring the fringes contrast as a function of the interferometer delay (see Fig. SI 4b). The strong background of 20% is due to residual scattered laser. The experimental results are fitted by the  $g^{(1)}$  function of a two-level system, given by Eq. 1 (see Methods of the main paper), and the deduced coherence time is  $T_2 = 0.5 \pm 0.05$  ns. The two panels correspond to two different excitation powers. In particular, on the bottom panel, the Rabi oscillations that the two-level system undergoes when it is strongly coupled to the resonant laser above saturation are observable. The experimental value

of  $T_2$  reproduces accurately the data from the whole set of measurements performed for several excitation powers (not shown here). Moreover, the combination of the measured  $T_1$  and  $T_2$  describes reliably all the HBT and HOM measurements, raising a high level of confidence about these values.

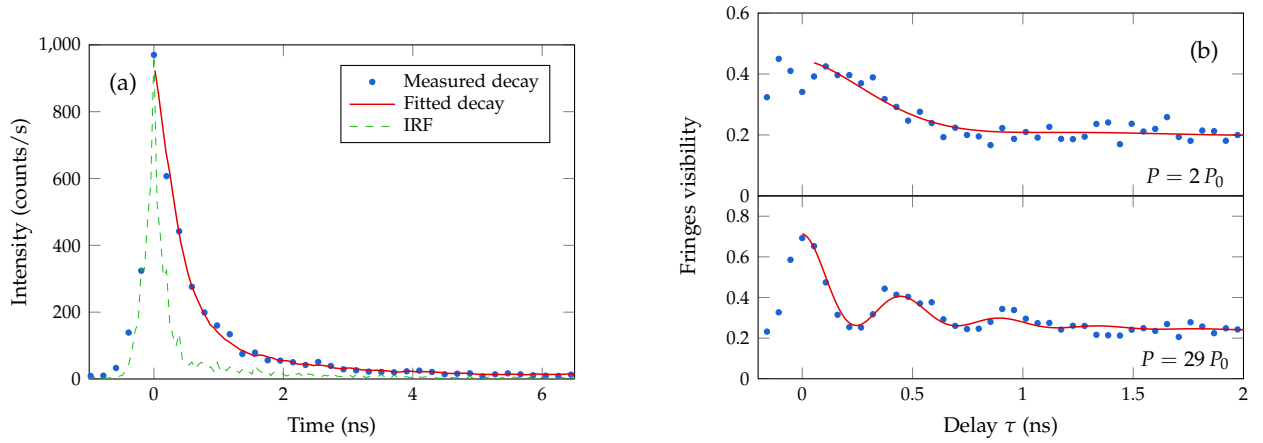


FIGURE SI 4 | **Dynamical properties of the quantum dot emission.** **a**,  $T_1$  measurement: the experimental decay curve (blue dots) is presented with a fit (red solid line) of an exponential decay with a time constant  $T_1 = 0.34 \pm 0.05$  ns, convoluted by the Instrument Response Function (dashed green line). **b**,  $T_2$  measurement: fringes visibility as a function of the interferometer delay (blue dots), fitted by the  $g^{(1)}$  function of a two-level system (see Eq. 1 in Methods of the main paper) (red solid line). The excitation power is  $P = 2P_0$  for the top panel and  $P = 29P_0$  for the bottom panel.  $T_1 = 0.3$  ns for both. The extracted value of the coherence time is  $T_2 = 0.5 \pm 0.05$  ns.

## References

- <sup>1</sup> A. Lebreton, I. Abram, R. Braive, I. Sagnes, I. Robert-Philip & A. Beveratos, *Unequivocal Differentiation of Coherent and Chaotic Light through Interferometric Photon Correlation Measurements*, Phys. Rev. Lett. **110**, 163603 (2013).
- <sup>2</sup> O. Svelto, *Principles of Lasers*, Plenum Press, New York, 1998.
- <sup>3</sup> H. S. Nguyen, G. Sallen, C. Voisin, Ph. Roussignol, C. Diederichs & G. Cassabois, *Ultra-coherent single photon source*, Appl. Phys. Lett. **99**, 261904 (2011).
- <sup>4</sup> L. Mandel, *Quantum effects in one-photon and two-photon interference*, Rev. Mod. Phys. **71**, S274–S282 (1999).
- <sup>5</sup> T. B. Pittman, D. V. Strekalov, A. Migdall, M. H. Rubin, A. V. Sergienko & Y. H. Shih, *Can Two-Photon Interference be Considered the Interference of Two Photons?* Phys. Rev. Lett. **77**, 1917 (1996).